Transmission Model of Partial Discharges on Medium Voltage Cables

Martin Fritsch, *Student Member, IEEE*, and Martin Wolter, *Senior Member, IEEE*

***Abstract*—Medium voltage cables are poor transmitters of signals with high frequency spectrum such as partial discharges. The propagating signals are strongly attenuated and distorted depending on the transmitted distance. In order to understand this process, this article provides a model to simulate the transmission of such signals on medium voltage cables. Compared to earlier approaches, this model does not neglect the wave character of the high frequency signals. Therefore, to describe the signal transmission, a comprehensible solution of the telegrapher's equations is provided. To work with this solution, the propagation constant of the medium voltage cable used must also be known. This propagation constant is calculated on the basis of the individual cable layers, considering all ohmic and dielectric losses. In contrast to previous methods, all primary line constants are modeled frequency dependent. The final transmission model is able to predict the spectrum of a transmitted signal at any distance from its origin. Validation measurements show that prediction and measurement agree with good accuracy. A possible application of the developed model is the investigation of the transmission of partial discharges on medium voltage cables. This model is probably also suitable for high voltage cables.**

***Index Terms*—Attenuation, cable model, high-frequency, partial discharges, power cables, propagation constant, transmission lines, transmission model, XLPE.**

I. Introduction

PARTIAL discharges (PD) are small dielectric breakdowns within an electrical insulation system. They can occur localized at any defective points in the insulation. In contrast to the short circuit, the space between the two conductors is not completely bridged by the discharge. Thus, PD activity can last for a while and successively damage the insulation. They mainly occur on the operating equipment of electrical power transmission systems under high-voltage stresses. By measuring the PD, defects can be detected in time and power outages can be avoided.

The discharge manifests itself as a transient electromagnetic pulse. The pulse width is usually in the range of a few nanoseconds. In the frequency domain, such nanosecond pulses consist of a wide spectrum of frequencies from 0 Hz to tens of MHz. The shorter the pulse duration is, the wider the corresponding frequency spectrum becomes. The maximum frequency component of most PD should be in the range of 3–100 MHz, which corresponds to the high-frequency (HF) and lower very-high-frequency (VHF) range. When HF signals are mentioned in the following article, this frequency range is meant.

The broadband PD pulses usually have to propagate from their point of origin to a measuring device via a transmission line (TL), e.g. overhead lines or power cables. This propagation distorts the initial impulse and reduces the bandwidth of the measurable spectrum depending on the distance traveled. To model and simulate this process, a complete understanding of the propagation behavior of the TL used is necessary. A suitable model can then describe the transmission of PD, as well as all other HF signals, on the TL. In this article such a model is presented, where power cables are used as TL. The investigations are carried out using a medium-voltage (MV) cable with a nominal voltage of 20 kV. This cable is representative of all MV cables of different voltage levels, as their structure is always very similar.

Most publications on this signal transmission topic have not considered the TL theory, e.g. [1]–[4]. To correctly model the transmission of PD or other HF signals on a TL, a solution of the telegrapher's equations is required. These wave equations are not negligible if the wavelength of the transmitted signal becomes smaller than the length of the TL. This is almost always the case with signals like PD. To close this research gap, this article gives a solution of the telegrapher's equations, which describes the transmission of a PD along a TL. Similar approaches were published in [5], [6]. However, both publications have shortcomings in the derivation of their solution. More precisely, both solutions show a discrepancy in their right-sided voltage equation. Furthermore, they are not comprehensible because the authors do not provide a detailed derivation. These deficiencies are addressed in this work.

The quality of the signal transmission depends mainly on the MV cable used or its propagation constant. In contrast to telecommunication coaxial cables, power cables are optimized for power transmission at 50 Hz under high voltage conditions. Therefore, the cable construction contains additional semiconducting layers for field control, which have a significant attenuating effect especially on HF signals. These layers must be considered in order to correctly model the propagation constant of an power cable. Despite the many publications on this topic, e.g. [1]–[7], a purely analytical, comprehensive and reproducible

Manuscript received October 29, 2020; revised January 11, 2021; accepted February 18, 2021. Date of publication February 23, 2021; date of current version January 24, 2022. This work was supported by the European Regional Development Fund under Project Low Cost Teilentladungsmessung (ZS/2018/12/96267). Paper no. TPWRD-01588-2020. *(Corresponding author: Martin Fritsch.)*

The authors are with the Institute of Electric Power Systems, Otto von Guericke University, D-39106 Magdeburg, Germany (e-mail: martin.fritsch@ovgu.de; martin.wolter@ovgu.de).

Color versions of one or more figures in this article are available at https://doi.org/10.1109/TPWRD.2021.3061201.

Digital Object Identifier 10.1109/TPWRD.2021.3061201

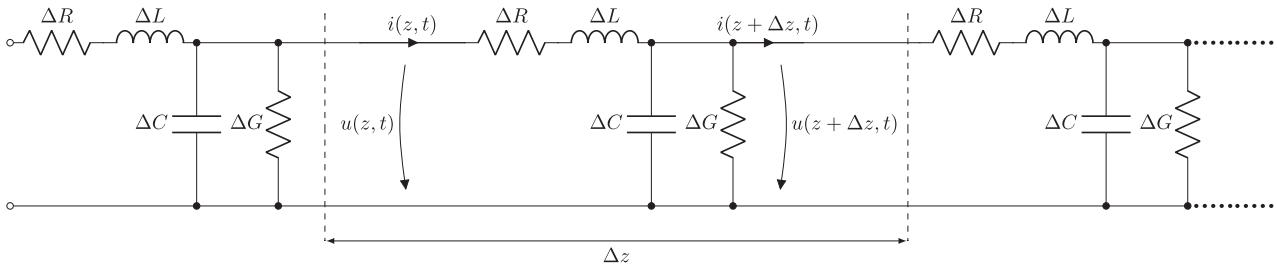

Fig. 1. Distributed-element model of a TL.

method for calculating the propagation constant of an MV cable is still missing. Thus, this article aims to provide such a method. The shown calculation of the propagation constant of an MV cable is mainly based on the work of [7]–[9] and combines and extends their results. The frequency dependence of all electrical parameters is considered. Neglecting these frequency dependencies is inaccurate for the transmitted HF signals.

The transmission model is derived in three sections and is then validated. In Section II the solution of the telegrapher's equations is derived. Section III deals with the propagation constant of MV cables. Section IV contains the modeling of PD pulses. Section V shows how to use the final transmission model and provides example measurements for its validation.

II. Transmission Model

The shortest wavelengths in the spectrum of PD or similar signals with HF spectrum are usually shorter than their transmitting line, e.g. 30 MHz corresponds to a wavelength of $\lambda \approx 10\,\mathrm{m}$. Therefore, the TL theory with its wave equations must be applied.

A. Derivation of the Telegrapher's Equations

It is assumed that the material and structure of a TL are homogeneous along its length. Therefore, the equivalent circuit of the TL can be divided into infinitesimal small equal elements of length Δz, see Fig. 1. Each segment of this distributed-element model is then characterized as follows:

$$R' = \frac{\Delta R}{\Delta z}\ \text{in}\ \frac{\Omega}{\mathrm{m}} \qquad L' = \frac{\Delta L}{\Delta z}\ \text{in}\ \frac{\mathrm{H}}{\mathrm{m}} \tag{1}$$

$$G' = \frac{\Delta G}{\Delta z}\ \text{in}\ \frac{\mathrm{S}}{\mathrm{m}} \qquad C' = \frac{\Delta C}{\Delta z}\ \text{in}\ \frac{\mathrm{F}}{\mathrm{m}} \tag{2}$$

These four electrical parameters are called primary line constants. They are sufficient to fully characterize any conductive TL. Contrary to their name they are not constant, but frequency dependent $R'(\omega)$, $L'(\omega)$, $C'(\omega)$ and $G'(\omega)$. For better readability, the frequency dependence is not marked in the remaining text.

The telegrapher's equations are derived from Fig. 1. For a more detailed derivation see [10], [11]. The application of Kirchhoff's voltage law with $\Delta z \to 0$ leads to:

$$-\frac{\partial u(z,t)}{\partial z} = R' \cdot i(z,t) + L' \cdot \frac{\partial i(z,t)}{\partial t} \tag{3}$$

The application of Kirchhoff's current law with $\Delta z \to 0$ leads to:

$$-\frac{\partial i(z,t)}{\partial z} = G' \cdot u(z,t) + C' \cdot \frac{\partial u(z,t)}{\partial t} \tag{4}$$

The two coupled, linear partial differential equations (3) and (4) are the telegrapher's equations in the time domain.

If only stationary signals are considered, a further simplification can be achieved by transforming these equations into the frequency domain. Voltage and current signals are then represented as a superposition of many sinusoidal signals with different frequencies. Since all time information in the frequency domain is lost, this approach is not suitable for the investigation of transient events. But it can be used if only the transmission behavior of the TL shall be investigated.

Sine functions can be formulated in the phasor notation with RMS magnitudes:

$$u(z,t) = \sqrt{2}\,U(z)\,\cos(\omega t + \varphi_\mathrm{U}) = \sqrt{2}\ \mathrm{Re}\left(\underline{U}(z)\,\mathrm{e}^{\mathrm{j}\omega t}\right) \tag{5}$$

$$i\,(z,t) = \sqrt{2}\ I(z)\,\cos(\omega t + \varphi_\mathrm{I}) = \sqrt{2}\ \mathrm{Re}\left(\underline{I}\,(z)\,\mathrm{e}^{\mathrm{j}\omega t}\right) \tag{6}$$

where $\underline{U}(z) = U(z)\,\mathrm{e}^{\mathrm{j}\varphi_\mathrm{U}}$ and $\underline{I}(z) = I(z)\,\mathrm{e}^{\mathrm{j}\varphi_\mathrm{I}}$. The transformation of (3) and (4) into the frequency domain then yields:

$$-\frac{\partial \underline{U}(z)}{\partial z} = (R' + \mathrm{j}\omega L')\ \underline{I}\,(z) = \underline{Z}'(\omega)\,\underline{I}\,(z) \tag{7}$$

$$-\frac{\partial \underline{I}\,(z)}{\partial z} = (G' + \mathrm{j}\omega C')\,\underline{U}(z) = \underline{Y}'(\omega)\,\underline{U}(z) \tag{8}$$

$\underline{Z}'(\omega)$ is the complex series impedance per unit length in $\frac{\Omega}{\mathrm{m}}$ and $\underline{Y}'(\omega)$ is the complex shunt admittance per unit length in $\frac{\mathrm{S}}{\mathrm{m}}$. The frequency dependence of series impedance and shunt admittance is not marked in the remaining text. The same applies for the later mentioned secondary line constants $\underline{\gamma}$, α, β, $\underline{Z}_\mathrm{c}$ and $\underline{r}_\mathrm{z}$, which are all frequency dependent too.

Deriving (7) and (8) with respect to z and mutual substitution leads to the telegrapher's equations in the frequency domain:

$$\frac{\partial^2 \underline{U}(z)}{\partial z^2} = \underline{Z}'\,\underline{Y}'\,\underline{U}(z) = \underline{\gamma}^2\,\underline{U}(z) \tag{9}$$

$$\frac{\partial^2 \underline{I}\,(z)}{\partial z^2} = \underline{Z}'\ \underline{Y}'\ \underline{I}\,(z) = \underline{\gamma}^2\,\underline{I}\,(z) \tag{10}$$

Two complex wave equations (9) and (10) are obtained, where $\underline{\gamma}$ is the propagation constant of the TL, which can be split into the attenuation constant α in $\frac{\mathrm{Np}}{\mathrm{m}}$ and the phase constant β in $\frac{\mathrm{rad}}{\mathrm{m}}$:

$$\underline{\gamma} = \sqrt{\underline{Z}'\,\underline{Y}'} = \sqrt{(R' + \mathrm{j}\omega L')\,(G' + \mathrm{j}\omega C')} = \alpha + \mathrm{j}\beta \tag{11}$$

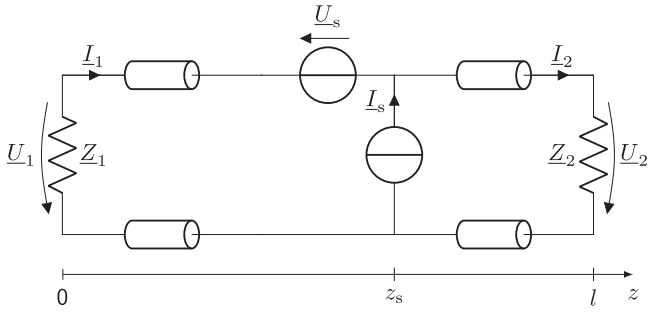

Fig. 2. Terminated TL with PD at any point z_s along its length l.

The conversion from neper to decibel is $1\,\mathrm{Np} \approx 8.686\,\mathrm{dB}$. Using an MV cable as TL, $\underline{\gamma}$ can be determined as described in Section III.

B. General Solution of Telegrapher's Equations

The general solution of (9) and (10) is:

$$\underline{U}(z) = \underline{U}_\mathrm{f}\,\mathrm{e}^{-\underline{\gamma}z} + \underline{U}_\mathrm{b}\,\mathrm{e}^{\underline{\gamma}z} \tag{12}$$

$$\underline{I}(z) = \underline{I}_\mathrm{f}\,\mathrm{e}^{-\underline{\gamma}z} + \underline{I}_\mathrm{b}\,\mathrm{e}^{\underline{\gamma}z} \tag{13}$$

Physically, this solution can be interpreted as the sum of a forward and a backward traveling wave. The constants $\underline{U}_\mathrm{f}$ and $\underline{U}_\mathrm{b}$ are the phasors of the forward and backward voltage wave in V. The constants $\underline{I}_\mathrm{f}$ and $\underline{I}_\mathrm{b}$ are the phasors of the forward and backward current wave in A. They are determined by the boundary conditions of the problem to be solved [10].

C. Relationship Between Individual Waves

Voltage and current waves are related to each other via $\underline{Z}_\mathrm{c}$:

$$\underline{Z}_\mathrm{c} = \frac{\underline{U}_\mathrm{f}}{\underline{I}_\mathrm{f}} = -\frac{\underline{U}_\mathrm{b}}{\underline{I}_\mathrm{b}} = \sqrt{\frac{\underline{Z}'}{\underline{Y}'}} \tag{14}$$

where $\underline{Z}_\mathrm{c}$ is the characteristic impedance of the TL in Ω [10].

Backward and forward traveling waves are related to each other via $\underline{r}_\mathrm{z}$:

$$\frac{\underline{U}_\mathrm{b}\,\mathrm{e}^{\underline{\gamma}z}}{\underline{U}_\mathrm{f}\,\mathrm{e}^{-\underline{\gamma}z}} = \frac{\frac{\underline{U}(z)}{\underline{I}(z)} - \underline{Z}_\mathrm{c}}{\frac{\underline{U}(z)}{\underline{I}(z)} + \underline{Z}_\mathrm{c}} = \frac{\underline{Z}_\mathrm{z} - \underline{Z}_\mathrm{c}}{\underline{Z}_\mathrm{z} + \underline{Z}_\mathrm{c}} = \underline{r}_\mathrm{z} \tag{15}$$

where $\underline{r}_\mathrm{z}$ is the reflection coefficient at the position z. It depends on the impedance $\underline{Z}_\mathrm{z}$ at this location and indicates which portion of a forward traveling wave is reflected back into the TL [11].

D. Solution for the Transmission of a PD Along a TL

Fig. 2 shows a TL of finite length l with arbitrary termination impedances $\underline{Z}_1$ and $\underline{Z}_2$ at both ends. A PD (or any other signal with HF spectrum) can occur at any point $0 \le z_s \le l$ along the TL. It can be modeled with the following consideration. In the time domain it is possible to measure either directly the current of a PD pulse or its voltage. Accordingly, a PD can be considered in the model as a voltage or current source. To include both options, the PD is modeled in the frequency domain by both sources at its point of origin z_s. Which representation is used depends on the available measurement data. The values of $\underline{U}_s$ or $\underline{I}_s$ for each frequency component are then determined by the measured voltage or current density spectrum of the initial PD pulse. Further details on the use of this model follow in Section IV.

One part of the TL is on the left of the PD $z < z_s$ and the other part on the right $z > z_s$. The general solution of the telegrapher's equation in the frequency domain (12) and (13) applies to both parts individually. Setting up the initial system of equations under further consideration of (14):

$$\left.\begin{aligned}\underline{U}_1(z) &= \underline{U}_{\mathrm{f},1}\,\mathrm{e}^{-\underline{\gamma}z} + \underline{U}_{\mathrm{b},1}\,\mathrm{e}^{\underline{\gamma}z}\\ \underline{I}_1(z) &= \frac{\underline{U}_{\mathrm{f},1}}{\underline{Z}_\mathrm{c}}\,\mathrm{e}^{-\underline{\gamma}z} - \frac{\underline{U}_{\mathrm{b},1}}{\underline{Z}_\mathrm{c}}\,\mathrm{e}^{\underline{\gamma}z}\end{aligned}\right\} z < z_\mathrm{s} \tag{16}$$

$$\left.\begin{aligned}\underline{U}_2(z) &= \underline{U}_{\mathrm{f},2}\,\mathrm{e}^{-\underline{\gamma}z} + \underline{U}_{\mathrm{b},2}\,\mathrm{e}^{\underline{\gamma}z}\\ \underline{I}_2(z) &= \frac{\underline{U}_{\mathrm{f},2}}{\underline{Z}_\mathrm{c}}\,\mathrm{e}^{-\underline{\gamma}z} - \frac{\underline{U}_{\mathrm{b},2}}{\underline{Z}_\mathrm{c}}\,\mathrm{e}^{\underline{\gamma}z}\end{aligned}\right\} z > z_\mathrm{s} \tag{17}$$

Four boundary conditions are required to solve this system. Two are obtained from the termination impedances of the TL:

$$\underline{U}_1(0) = -\underline{Z}_1\,\underline{I}_1(0) \tag{18}$$

$$\underline{U}_2(l) = \underline{Z}_2\,\underline{I}_2(l) \tag{19}$$

The other two are obtained by the transition condition at z_s:

$$\underline{I}_1(z_\mathrm{s}) + \underline{I}_\mathrm{s} = \underline{I}_2(z_\mathrm{s}) \tag{20}$$

$$\underline{U}_1(z_\mathrm{s}) + \underline{U}_\mathrm{s} = \underline{U}_2(z_\mathrm{s}) \tag{21}$$

Now the initial system of equations can be solved for the given boundary conditions. At first a detailed formulation of the boundary conditions with (16) and (17) can be given:

$$\underline{U}_{\mathrm{f},1} + \underline{U}_{\mathrm{b},1} = -\underline{Z}_1\left(\frac{\underline{U}_{\mathrm{f},1}}{\underline{Z}_\mathrm{c}} - \frac{\underline{U}_{\mathrm{b},1}}{\underline{Z}_\mathrm{c}}\right) \tag{22}$$

$$\underline{U}_{\mathrm{f},2}\,\mathrm{e}^{-\underline{\gamma}l} + \underline{U}_{\mathrm{b},2}\,\mathrm{e}^{\underline{\gamma}l} = \underline{Z}_2\left(\frac{\underline{U}_{\mathrm{f},2}}{\underline{Z}_\mathrm{c}}\,\mathrm{e}^{-\underline{\gamma}l} - \frac{\underline{U}_{\mathrm{b},2}}{\underline{Z}_\mathrm{c}}\,\mathrm{e}^{\underline{\gamma}l}\right) \tag{23}$$

$$\frac{\underline{U}_{\mathrm{f},1}}{\underline{Z}_\mathrm{c}}\,\mathrm{e}^{-\underline{\gamma}z_\mathrm{s}} - \frac{\underline{U}_{\mathrm{b},1}}{\underline{Z}_\mathrm{c}}\,\mathrm{e}^{\underline{\gamma}z_\mathrm{s}} + \underline{I}_\mathrm{s} = \frac{\underline{U}_{\mathrm{f},2}}{\underline{Z}_\mathrm{c}}\,\mathrm{e}^{-\underline{\gamma}z_\mathrm{s}} - \frac{\underline{U}_{\mathrm{b},2}}{\underline{Z}_\mathrm{c}}\,\mathrm{e}^{\underline{\gamma}z_\mathrm{s}} \tag{24}$$

$$\underline{U}_{\mathrm{f},1}\,\mathrm{e}^{-\underline{\gamma}z_\mathrm{s}} + \underline{U}_{\mathrm{b},1}\,\mathrm{e}^{\underline{\gamma}z_\mathrm{s}} + \underline{U}_\mathrm{s} = \underline{U}_{\mathrm{f},2}\,\mathrm{e}^{-\underline{\gamma}z_\mathrm{s}} + \underline{U}_{\mathrm{b},2}\,\mathrm{e}^{\underline{\gamma}z_\mathrm{s}} \tag{25}$$

Solving (22) for the forward voltage phasor $\underline{U}_{\mathrm{f},1}$ of the left TL section:

$$\underline{U}_{\mathrm{f},1} = \underline{U}_{\mathrm{b},1}\left(\frac{\underline{Z}_1 - \underline{Z}_\mathrm{c}}{\underline{Z}_1 + \underline{Z}_\mathrm{c}}\right) = \underline{U}_{\mathrm{b},1}\,\underline{r}_1 \tag{26}$$

Solving (23) for the backward voltage phasor $\underline{U}_{\mathrm{b},2}$ of the right TL section:

$$\underline{U}_{\mathrm{b},2} = \underline{U}_{\mathrm{f},2}\left(\frac{\underline{Z}_2 - \underline{Z}_\mathrm{c}}{\underline{Z}_2 + \underline{Z}_\mathrm{c}}\right)\mathrm{e}^{-2\underline{\gamma}l} = \underline{U}_{\mathrm{f},2}\,\underline{r}_2\,\mathrm{e}^{-2\underline{\gamma}l} \tag{27}$$

Solving (24) for the backward voltage phasor $\underline{U}_{\mathrm{b},1}$ of the left TL section:

$$\underline{U}_{\mathrm{b},1} = \underline{U}_{\mathrm{f},1}\,\mathrm{e}^{-2\underline{\gamma}z_\mathrm{s}} - \underline{U}_{\mathrm{f},2}\,\mathrm{e}^{-2\underline{\gamma}z_\mathrm{s}} + \underline{U}_{\mathrm{b},2} + \underline{I}_\mathrm{s}\,\underline{Z}_\mathrm{c}\,\mathrm{e}^{-\underline{\gamma}z_\mathrm{s}} \tag{28}$$

Solving (25) for the forward voltage phasor $\underline{U}_{\mathrm{f},2}$ of the right TL section:

$$\underline{U}_{\mathrm{f},2} = \underline{U}_{\mathrm{f},1} + \underline{U}_{\mathrm{b},1}\,\mathrm{e}^{2\underline{\gamma}z_\mathrm{s}} - \underline{U}_{\mathrm{b},2}\,\mathrm{e}^{2\underline{\gamma}z_\mathrm{s}} + \underline{U}_\mathrm{s}\,\mathrm{e}^{\underline{\gamma}z_\mathrm{s}} \tag{29}$$

Substituting (26) and (27) into (28):

$$\underline{U}_{\mathrm{b},1} = \frac{\underline{U}_{\mathrm{f},2}\,(\underline{r}_2\,\mathrm{e}^{-2\underline{\gamma}l} - \mathrm{e}^{-2\underline{\gamma}z_\mathrm{s}}) + \underline{I}_\mathrm{s}\,\underline{Z}_\mathrm{c}\,\mathrm{e}^{-\underline{\gamma}z_\mathrm{s}}}{1 - \underline{r}_1\,\mathrm{e}^{-2\underline{\gamma}z_\mathrm{s}}} \tag{30}$$

Substituting (26) and (27) into (29):

$$\underline{U}_{\mathrm{f},2} = \frac{\underline{U}_{\mathrm{b},1}\,(\underline{r}_1 + \mathrm{e}^{2\underline{\gamma}z_\mathrm{s}}) + \underline{U}_\mathrm{s}\,\mathrm{e}^{\underline{\gamma}z_\mathrm{s}}}{1 + \underline{r}_2\,\mathrm{e}^{-2\underline{\gamma}l}\,\mathrm{e}^{2\underline{\gamma}z_\mathrm{s}}} \tag{31}$$

Now substituting (30) into (31) and again solve for $\underline{U}_{\mathrm{f},2}$:

$$\underline{U}_{\mathrm{f},2} = \frac{1}{2}\,\frac{(\underline{U}_\mathrm{s} + \underline{I}_\mathrm{s}\,\underline{Z}_\mathrm{c})\,\mathrm{e}^{\underline{\gamma}z_\mathrm{s}} - (\underline{U}_\mathrm{s} - \underline{I}_\mathrm{s}\,\underline{Z}_\mathrm{c})\,\underline{r}_1\,\mathrm{e}^{-\underline{\gamma}z_\mathrm{s}}}{1 - \underline{r}_1\,\underline{r}_2\,\mathrm{e}^{-2\underline{\gamma}l}} \tag{32}$$

And finally substituting (31) into (30) and solve for $\underline{U}_{\mathrm{b},1}$:

$$\underline{U}_{\mathrm{b},1} = \frac{\mathrm{e}^{-\underline{\gamma}l}}{2}\,\frac{(\underline{U}_\mathrm{s} + \underline{I}_\mathrm{s}\,\underline{Z}_\mathrm{c})\,\underline{r}_2\,\mathrm{e}^{-\underline{\gamma}(l-z_\mathrm{s})} - (\underline{U}_\mathrm{s} - \underline{I}_\mathrm{s}\,\underline{Z}_\mathrm{c})\,\mathrm{e}^{\underline{\gamma}(l-z_\mathrm{s})}}{1 - \underline{r}_1\,\underline{r}_2\,\mathrm{e}^{-2\underline{\gamma}l}} \tag{33}$$

The four initially unknown phasors of the equation system are now known for the given boundary conditions. Thus, (26), (27), (32) and (33) can now be used to write the final solution of the initial system of equations. For $z < z_\mathrm{s}$ yields:

$$\begin{aligned}\underline{U}_1(z) = {} & \frac{\mathrm{e}^{-\underline{\gamma}l}(\mathrm{e}^{\underline{\gamma}z} + \underline{r}_1\mathrm{e}^{-\underline{\gamma}z})}{2\left(1 - \underline{r}_1\underline{r}_2\mathrm{e}^{-2\underline{\gamma}l}\right)}\left[\left(\underline{r}_2\mathrm{e}^{-\underline{\gamma}(l-z_\mathrm{s})} - \mathrm{e}^{\underline{\gamma}(l-z_\mathrm{s})}\right)\underline{U}_\mathrm{s}\right. \\ & \left. + \left(\underline{r}_2\mathrm{e}^{-\underline{\gamma}(l-z_\mathrm{s})} + \mathrm{e}^{\gamma(l-z_\mathrm{s})}\right)\underline{I}_\mathrm{s}\underline{Z}_\mathrm{c}\right] \\ \underline{I}_1(z) = {} & \frac{\mathrm{e}^{-\underline{\gamma}l}(-\mathrm{e}^{\underline{\gamma}z} + \underline{r}_1\mathrm{e}^{-\underline{\gamma}z})}{2\left(\underline{Z}_\mathrm{c}(1 - \underline{r}_1\underline{r}_2\mathrm{e}^{-2\underline{\gamma}l})\right)}\left[\left(\underline{r}_2\mathrm{e}^{-\underline{\gamma}(l-z_\mathrm{s})} - \mathrm{e}^{\underline{\gamma}(l-z_\mathrm{s})}\right)\underline{U}_\mathrm{s}\right. \\ & \left. + \left(\underline{r}_2\mathrm{e}^{-\underline{\gamma}(l-z_\mathrm{s})} + \mathrm{e}^{\underline{\gamma}(l-z_\mathrm{s})}\right)\underline{I}_\mathrm{s}\underline{Z}_\mathrm{c}\right]\end{aligned} \tag{34}$$

And finally, for the right-side $z > z_\mathrm{s}$ yields:

$$\begin{aligned}\underline{U}_2(z) = {} & \frac{\mathrm{e}^{-\underline{\gamma}l}(\mathrm{e}^{\underline{\gamma}(l-z)} + \underline{r}_2\mathrm{e}^{-\underline{\gamma}(l-z)})}{2\left(1 - \underline{r}_1\underline{r}_2\mathrm{e}^{-2\underline{\gamma}l}\right)}\left[\left(\mathrm{e}^{\underline{\gamma}z_\mathrm{s}} - \underline{r}_1\mathrm{e}^{-\underline{\gamma}z_\mathrm{s}}\right)\underline{U}_\mathrm{s}\right. \\ & \left. + \left(\mathrm{e}^{\underline{\gamma}z_\mathrm{s}} + \underline{r}_1\mathrm{e}^{-\gamma z_\mathrm{s}}\right)\underline{I}_\mathrm{s}\underline{Z}_\mathrm{c}\right] \\ \underline{I}_2(z) = {} & \frac{\mathrm{e}^{-\underline{\gamma}l}(\mathrm{e}^{\underline{\gamma}(l-z)} - \underline{r}_2\mathrm{e}^{-\underline{\gamma}(l-z)})}{2\left(\underline{Z}_\mathrm{c}(1 - \underline{r}_1\underline{r}_2\mathrm{e}^{-2\underline{\gamma}l})\right)}\left[\left(\mathrm{e}^{\underline{\gamma}z_\mathrm{s}} - \underline{r}_1\mathrm{e}^{-\underline{\gamma}z_\mathrm{s}}\right)\underline{U}_\mathrm{s}\right. \\ & \left. + \left(\mathrm{e}^{\underline{\gamma}z_\mathrm{s}} + \underline{r}_1\mathrm{e}^{-\underline{\gamma}z_\mathrm{s}}\right)\underline{I}_\mathrm{s}\underline{Z}_\mathrm{c}\right]\end{aligned} \tag{35}$$

With this solution the voltage and current distribution on both sides of the PD can be calculated for a known TL. The solution depends only on the arbitrary source signal $\underline{U}_\mathrm{s}$ or $\underline{I}_\mathrm{s}$. Only one of the two sources is used at a time and the other is set to zero.

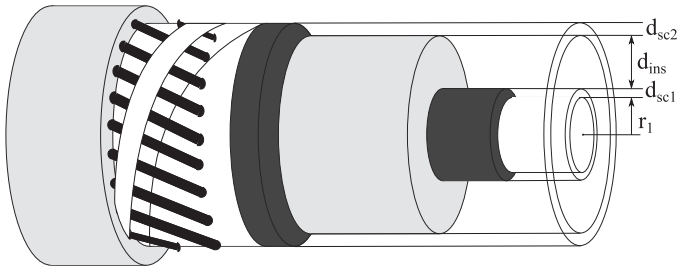

Fig. 3. Cross-section through a typical single-phase MV cable.

III. Propagation Constant of a Power Cable

To use the derived solution, the propagation constant $\underline{\gamma}$ of the TL must be known. For the present work, a common cross-linked polyethylene (XLPE) power cable should be used as TL. In this section, the calculation of $\underline{\gamma}$ for such a cable is derived step by step. At the end of the section, $\underline{\gamma}$ is calculated for an example cable and validated by measurements. An MV cable is used for this purpose.

As shown in Fig. 3, power cables typically consist of an inner conductor with radius r_1, an inner semiconducting layer or conductor screen of thickness d_{sc1}, a dielectric insulation layer of thickness d_{ins}, an outer semiconducting layer or insulation screen of thickness d_{sc2}, an outer conductor with inner radius $r_2 = r_1 + d_{\mathrm{sc1}} + d_{\mathrm{ins}} + d_{\mathrm{sc2}}$ and an outer protective sheath. In addition, power cables may have an additional thin, water-swellable semiconducting tape layer between insulation screen and outer conductor. However, such a layer is not included in the example MV cable examined later. The semiconducting layers are used to provide a smooth interface between the conductors and the insulating layer. This serves to homogenize the electric field and avoid highly stressed areas due to small surface imperfections at the interfaces of the conductors.

To calculate $\underline{\gamma}$, first the primary line constants R', L', C' and G' must be determined. It is assumed that the cable geometry is constant over the entire length. To simplify the calculations, the inner conductor is considered as a solid cylinder and the outer conductor as a solid hollow cylinder. It is also assumed that the cable is straight over its entire length. This implies a homogeneous field distribution and allows the calculation of the primary line constants [8].

A. Conductor Resistance

The resistance per unit length R' of a copper conductor at DC is calculated as follows:

$$R' = \frac{1}{\sigma_{\mathrm{co}} A} \tag{36}$$

where $\sigma_{\mathrm{co}} = 58.1395\,\frac{\mathrm{S}}{\mathrm{m}}$ is the electrical conductivity of the copper conductor and A is its cross-section in m^2. The resistance increases with frequency f due to the skin effect. The higher the frequency, the more current flows near the conductor surface. The thickness of this conductive layer is the skin depth δ in m

and can be calculated for metallic conductors according to:

$$\delta = \sqrt{\frac{2}{\sigma_{\mathrm{co}}\omega\mu_0\mu_{\mathrm{co}}}} \tag{37}$$

where $\mu_0 \approx 1.25\,664 \cdot 10^{-6}\ \frac{\mathrm{Vs}}{\mathrm{Am}}$ is the vacuum permeability, $\mu_{\mathrm{co}} = 1 - 6.4 \cdot 10^{-6} \approx 1$ is the relative permeability of copper and $\omega = 2\pi f$ is the angular frequency in $\frac{\mathrm{rad}}{\mathrm{s}}$. The skin depth δ indicates the depth, at which the current density $\vec{J}$ has decreased to $\frac{1}{\mathrm{e}}$ of its amplitude. In the MHz range, the skin depth for copper is only a few micrometers thick. Thus, the effective cross-section of the conductor is reduced at HF signals to about $A_{\mathrm{hf}} \approx 2\pi r\delta$. Then the conductor resistance can be calculated as follows [8]:

$$R' = \frac{1}{\sigma_{\mathrm{co}} A_{\mathrm{hf}}} \approx \frac{1}{\sigma_{\mathrm{co}} 2\pi r\delta} = \sqrt{\frac{\omega\mu_0\mu_{\mathrm{co}}}{2\sigma_{\mathrm{co}}}}\frac{1}{2\pi r} \tag{38}$$

The total resistance of a power cable is the sum of the resistances of the inner and outer conductor:

$$R' = \sqrt{\frac{\omega\mu_0\mu_{\mathrm{co}}}{2\sigma_{\mathrm{co}}}}\frac{1}{2\pi}\left(\frac{1}{r_1} + \frac{1}{r_2}\right) \tag{39}$$

B. Conductor Inductance

HF currents generate magnetic fields inside and outside the cable conductors. These magnetic fields change over time and induce an opposite voltage back into the conductors. This behavior is described by the conductor inductance per unit length L'. The influence of the magnetic fields on the conductors themselves, the so-called inner inductance L'_{i}, decreases with frequency due to the skin effect. Therefore, the inner inductance is negligible at frequencies $> 10\,\mathrm{kHz}$. Only the influence of the magnetic field between the conductors, the outer inductance L'_{o}, is relevant for calculating the total inductance of the TL in the HF range [8]:

$$L' \approx L'_{\mathrm{o}} = \frac{\mu_0\mu_{\mathrm{co}}}{2\pi}\ln\frac{r_2}{r_1} \tag{40}$$

C. Insulator Capacitance

The elements R' and L' describe the behavior of the conductors and C' and G' that of the dielectric material between the conductors. This dielectric consists of the main insulation layer and thin semiconducting layers on each side. Each of these layers has a frequency dependent capacitance per unit length C'. In general, the capacity of a coaxial cable layer can be calculated as follows [12], [13]:

$$\underline{C'} = \frac{2\pi\varepsilon_0\underline{\varepsilon}(\omega)}{\ln\left(\frac{r_2}{r_1}\right)} \tag{41}$$

where $\varepsilon_0 \approx 8.85\,418 \cdot 10^{-12}\ \frac{\mathrm{As}}{\mathrm{Vm}}$ is the vacuum permittivity and $\underline{\varepsilon}(\omega) = \varepsilon'(\omega) + \mathrm{j}\varepsilon''(\omega)$ is the permittivity of the dielectric layer. This permittivity describes the polarizability of the dielectric and is frequency dependent and complex.

The permittivity of the XLPE insulator layer can be assumed to be constant $\underline{\varepsilon}_{\mathrm{ins}} = 2.26 + \mathrm{j} \cdot 10^{-3}$ in the frequency range of interest [7], [9]. The permittivity of the semiconducting layers is usually not known from the datasheet of the power cable used.

TABLE I
PARAMETERS OF THE PERMITTIVITY MODEL OF THE SEMICONDUCTING CABLE LAYERS

Parameter	conductor screen	insulator screen	tape layer
A_1	105	95	160
A_2	50	90	48
α_1	0.5	0.3	0.5
α_2	0.3	0.5	0.7
τ_1	300 ns	100 ns	800 ns
τ_2	0.68 ns	4 ns	15 ns
ε_∞	4	2	1
σ_{DC}	0.15 $\frac{\mathrm{mS}}{\mathrm{m}}$	2.7 $\frac{\mathrm{mS}}{\mathrm{m}}$	32 $\frac{\mathrm{mS}}{\mathrm{m}}$

In [9], researchers made permittivity measurements for single-phase MV cables. The authors have fitted the following complex permittivity model to their measurements:

$$\underline{\varepsilon}(\omega) = \frac{A_1}{1 + (\mathrm{j}\omega\tau_1)^{(1-\alpha_1)}} + \frac{A_2}{1 + (\mathrm{j}\omega\tau_2)^{(1-\alpha_2)}} + \frac{\sigma_{\mathrm{DC}}}{\mathrm{j}\omega\varepsilon_0} + \varepsilon_\infty \tag{42}$$

A detailed description of this model and the measurement method can be found in the referenced article. The various parameters of the permittivity model are summarized in table I, separated by conductor screen and insulator screen. If necessary, the parameters of the optional water-swellable semiconducting tape layer are also added. With these data and (42) the permittivity of the two semiconducting layers are calculated.

Now the capacitance of each layer can be calculated according to (41):

$$\underline{C'}_{\mathrm{sc1}} = \frac{2\pi\varepsilon_0\underline{\varepsilon}_{\mathrm{sc1}}(\omega)}{\ln\left(\frac{r_1 + d_{\mathrm{sc1}}}{r_1}\right)} \tag{43}$$

$$\underline{C'}_{\mathrm{ins}} = \frac{2\pi\varepsilon_0\underline{\varepsilon}_{\mathrm{ins}}}{\ln\left(\frac{r_1 + d_{\mathrm{sc1}} + d_{\mathrm{ins}}}{r_1 + d_{\mathrm{sc1}}}\right)} \tag{44}$$

$$\underline{C'}_{\mathrm{sc2}} = \frac{2\pi\varepsilon_0\underline{\varepsilon}_{\mathrm{sc2}}(\omega)}{\ln\left(\frac{r_1 + d_{\mathrm{sc1}} + d_{\mathrm{ins}} + d_{\mathrm{sc2}}}{r_1 + d_{\mathrm{sc1}} + d_{\mathrm{ins}}}\right)} \tag{45}$$

The total insulator capacitance of a power cable results from all individual capacities in series:

$$\underline{C'} = \frac{1}{\frac{1}{\underline{C'}_{\mathrm{sc1}}} + \frac{1}{\underline{C'}_{\mathrm{ins}}} + \frac{1}{\underline{C'}_{\mathrm{sc2}}}} \tag{46}$$

If necessary, the capacitance of a possible water-swellable semiconducting tape layer is calculated and added in the same way.

D. Insulator Conductance

In XLPE cables, the influence of the insulator conductance per unit length G' is small compared to the dielectric losses due to polarization caused by $\underline{C'}$. The specific conductivity of the XLPE insulation material σ_{ins} is close to zero. The conductivities of the semiconducting layers are already considered in the used permittivity model. The XLPE conductance can therefore be

TABLE II
PARAMETERS OF THE MEDIUM VOLTAGE CABLE USED

Parameter	Value
Conductor material	Copper
Nominal voltage U_n	20 kV
Inner conductor cross-section	50 mm^2
Outer conductor cross-section	16 mm^2
r_1	4 mm
d_{sc1}	0.3 mm
d_{ins}	5.5 mm
d_{sc2}	0.6 mm
r_2	10.4 mm

neglected or, provided σ_{ins} is known, calculated as follows [13]:

$$G' = \frac{2\pi\sigma_{\mathrm{ins}}}{\ln\left(\frac{r_1+d_{\mathrm{sc1}}+d_{\mathrm{ins}}+d_{\mathrm{sc2}}}{r_1}\right)} \tag{47}$$

E. Secondary Line Constants

Now all primary line constants are determined for the specific power cable and the secondary line constants can be calculated. First the complex impedance of the TL can be calculated:

$$\underline{Z}' = R' + \mathrm{j}\omega L' \tag{48}$$

The complex admittance of the TL is:

$$\underline{Y}' = G' + \mathrm{j}\omega \underline{C}' \tag{49}$$

The propagation constant $\underline{\gamma}$ of the power cable can now be calculated according to (11). Finally, the characteristic impedance $\underline{Z}_\mathrm{c}$ of the TL can be calculated according to (14).

F. Validation of the Calculated Propagation Constant

To validate the calculation method shown, the propagation constant $\underline{\gamma}$ was calculated for an example MV cable. The cable type is N2XS2Y of Suedkabel GmbH. Some relevant parameters of this MV cable are listed in table II. The piece of cable used is $l = 10\,\mathrm{m}$ long. It should be mentioned that the cable length has no influence on $\underline{\gamma}$. It depends only on the cable geometry and material.

To validate the calculated $\underline{\gamma}$ of the MV cable, it is also measured with the help of a vector network analyzer (VNA). With the help of a VNA the scattering (S) parameters of a linear electrical network can be measured. Each TL can be interpreted as a linear two-port network. As VNA the model *DG8SAQ VNWA 3E* of SDR-Kits is used. With this device the S-parameters of the MV cable were measured from 0.1 to 250 MHz.

For the measurement, the MV cable must be connected to the transmit and receive SMA input of the VNA, see Fig. 4. Therefore, an adapter is required. For this purpose, an SMA cable is connected to each of the two VNA inputs. At the other cable ends, the inner and outer conductors are separated. They can now be soldered directly to the inner and outer conductors of the MV cable. Care must be taken to keep these unshielded cable sections as short as possible to avoid unwanted parasitic inductance in the network.

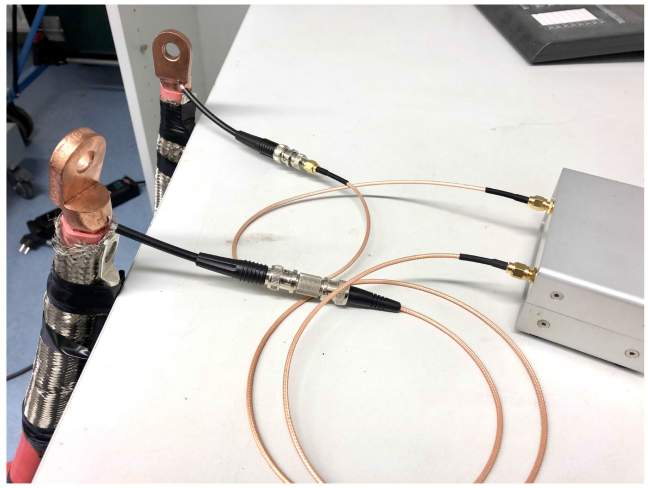

Fig. 4. Connection of the MV cable to the VNA. The MV cable is equipped with additional shielding at its end terminations to avoid parasitic inductance. In general, all unshielded sections should be avoided as much as possible.

Fig. 5. Adapter between VNA and MV cable and corresponding calibration scheme.

Before the measurement a correct SOLT-calibration of the VNA must be ensured according to Fig. 5. For this purpose, both adapters are connected to the VNA, but not to the MV cable. For *Short* calibration the adapter ends of the transmit input are soldered together. For *Load* calibration, a 50 Ω SMD resistor is soldered between the adapter ends of the transmit input. For *Through* calibration the adapter cables of both VNA inputs are soldered together. After successful calibration, the MV cable can be inserted exactly at the calibration plane according to Fig. 4 and the S-parameter measurement can be performed.

The relationship between the measured S-parameters and the propagation constant $\underline{\gamma}$ for a TL is [14], [15]:

$$\underline{\gamma} = \frac{1}{l}\cosh^{-1}\left(\frac{1-\underline{S}_{11}^2+\underline{S}_{21}^2}{2\underline{S}_{21}}\right) \tag{50}$$

Fig. 6 compares the analytical and measured propagation constant $\underline{\gamma}$ separated into its real part α and imaginary part β. The attenuation constant is converted to $\frac{\mathrm{dB}}{\mathrm{m}}$, see the comment to (11). Model and measurement of $\underline{\gamma}$ are very similar. From this it can be concluded that the propagation constant of the MV cable is determined correctly.

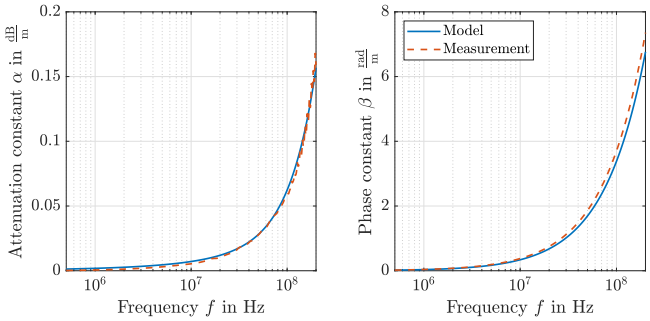

Fig. 6. Calculated and measured propagation constant of the MV cable.

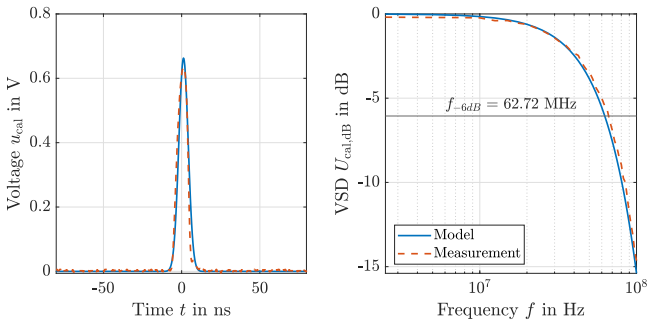

Fig. 7. PD calibrator 100 pC impulse in the time and frequency domain.

IV. Partial Discharge Model

In section II, a PD pulse was modeled with the help of a voltage source $\underline{U}_{\mathrm{s}}$ and a current source $\underline{I}_{\mathrm{s}}$ at location z_{s}, see Fig. 2. In this way it was achieved that both voltage or current measurements of a PD can be used as input of the model. Depending on which source is selected, the other is set to zero. Since we mainly measured voltages for this work, the voltage source $\underline{U}_{\mathrm{s}}$ will be used in the following. Thus, in our case $\underline{I}_{\mathrm{s}} = 0$.

The modeled PD sources $\underline{U}_{\mathrm{s}}$ or $\underline{I}_{\mathrm{s}}$ represent the initial PD signal, which is then transmitted on the power cable. They are the excitation of the system. This section shows, how this input variables of the transmission model can be determined.

For this work, a Haefely *KAL9511* PD generator was used to produce the required PD pulses. This calibrator can generate PD pulses with a fixed charge of 1 to 100 pC. To measure the voltage of such a pulse, the calibrator can be connected directly to the 50 Ω input channel of an oscilloscope. Then the circuit is impedance matched and the voltage pulse u_{cal} of the calibrator can be measured without occurring reflections. The red dashed line in the time domain of Fig. 7 shows the measured voltage of the 100 pC pulse, with an amplitude of $\hat{u}_{\mathrm{pd}} \approx 0.64\,\mathrm{V}$ and a pulse duration at half amplitude or full width at half maximum of $t_{\mathrm{FWHM}} \approx 8\,\mathrm{ns}$. The corresponding representation in the frequency domain shows the voltage spectral density (VSD) obtained by Fourier transformation $u_{\mathrm{cal}} \xrightarrow{\mathcal{F}} \underline{U}_{\mathrm{cal}}$ in $\frac{\mathrm{V}}{\mathrm{Hz}}$. For the figures, the VSD is converted into a logarithmic scale:

$$U_{\mathrm{cal,dB}} = 20\log_{10}\left(\frac{|\underline{U}_{\mathrm{cal}}|}{\max\left(|\underline{U}_{\mathrm{cal}}|\right)}\right),\ \text{in dB} \tag{51}$$

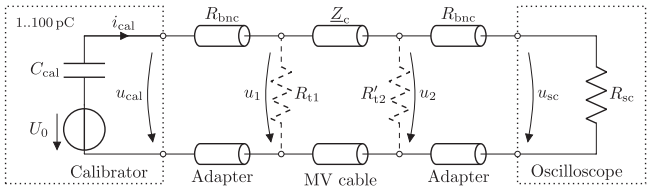

Fig. 8. Measurement setup for the first validation measurement of the transmission model.

The measured pulse consists mainly of frequency components up to the -6 dB cutoff-frequency $f_{-6\,\mathrm{dB}} \approx 62.72\,\mathrm{MHz}$. At this point the spectral amplitude has decreased by half. The shorter the pulse, the higher the -6 dB cutoff-frequency.

The measured PD voltage is similar to a symmetrical Gaussian function. Therefore, a PD in the time domain can be modeled by a Gaussian function:

$$u_{\mathrm{cal,m}}(t) = u_{\mathrm{cal,m}} = \hat{u}_{\mathrm{pd}}\,\mathrm{e}^{-\frac{(t-t_0)^2}{2c^2}} \tag{52}$$

where $t_0 = 0\,\mathrm{s}$ is the position of the peak center and c describes the pulse width. The relationship between t_{FWHM} and c is:

$$c = \frac{t_{\mathrm{FWHM}}}{2\sqrt{2\ln(2)}} \approx 0.42\,466\,t_{\mathrm{FWHM}} \tag{53}$$

The same PD model pulse in the frequency domain is [8]:

$$U_{\mathrm{cal,m}}(\omega) = U_{\mathrm{cal,m}} = \hat{u}_{\mathrm{pd}}\,c\,\sqrt{2\pi}\,\mathrm{e}^{-\frac{(c\,\omega)^2}{2}} \tag{54}$$

This obtained VSD can be used as input variable of the transmission model, i. e. as PD voltage source $\underline{U}_{\mathrm{s}}$. The PD current source is then set to $\underline{I}_{\mathrm{s}} = 0$.

Once again as a reminder. Instead of measuring the PD pulse voltage, the current could also be measured, e.g. with a current probe. Then $\underline{I}_{\mathrm{s}}$ would be determined in the same way and $\underline{U}_{\mathrm{s}} = 0$.

In order to fit this Gaussian pulse model to a specific voltage pulse measurement, the three free parameters $\hat{u}_{\mathrm{pd}}$, t_0 and c must be adjusted. The optimal parameter set is determined using an optimization algorithm that minimizes the sum of squared residuals. An example of the result can be seen in Fig. 7 as blue solid line. The Gaussian PD model can reproduce the measurement with sufficient accuracy.

V. Validation Measurements

To validate the final transmission model, measurements were made using the MV cable type described in Section III-F. For this purpose, two example measurements are shown in this section.

A. Measurement Setup With PD At the Beginning of the MV Cable

The measurement setup is shown in Fig. 8. An MV cable section with a length of $l = 10\,\mathrm{m}$ is connected on one side to the PD calibrator and on the other side to an oscilloscope. Thus, a PD pulse is injected at one end of the cable and the resulting voltage is measured at the other end. An oscilloscope with a bandwidth of 2 GHz and a sampling rate of 2.5 $\frac{\mathrm{GS}}{\mathrm{s}}$ is used. The transmitted

Fig. 9. PD calibrator with adapter cable for connection to the MV cable. R_{t1} can be soldered between the separated conductors if necessary. The oscilloscope was connected in a similar way, with optional R'_{t2}.

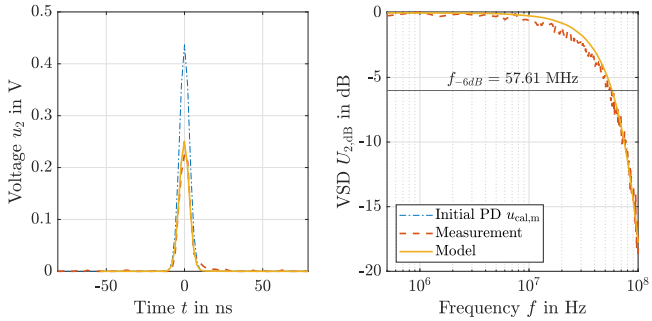

Fig. 10. 100 pC impulse after propagation on 10 m of MV cable in the time and frequency domain with $R_{t1} = 35\,\Omega$ and $R_{t2} = 50\,\Omega$.

voltage pulse u_2 is measured at an input channel with an input resistance of $R_{sc} = 50\,\Omega$. Passive probes on high-impedance input channels would falsify the HF measurements due to their capacitive behavior.

Adapters similar to those in Section III-F were used to connect the MV cable to the other devices, see Fig. 9. This time the adapters are made of BNC cable with a characteristic impedance of $R_{bnc} = 50\,\Omega$. One end is equipped with a BNC male connector. At the other end the inner and outer conductors are separated and can be soldered directly to the MV cable conductors. These unshielded cable sections of the adapter add a parasitic inductance to the measuring circuit. This could lead to unwanted low-pass behavior and thus to a falsified measurement. However, VNA measurements of the adapter's S-parameters show that this low-pass behavior is negligible up to 100 MHz if care is taken to keep the unshielded conductor section as short as possible ($\underline{S}_{11}$ is nearly constant). The adapters can therefore be considered as loss-free in the relevant frequency range. Thus, $u_{cal} \approx u_1$ and $u_{sc} \approx u_2$.

Optional SMD-resistors R_{t1} and R'_{t2} can be soldered between the two unshielded wires of the adapters to change the MV cable termination impedances:

$$\underline{Z}_1 = R_{t1} \tag{55}$$

$$\underline{Z}_2 = R_{t2} = R_{sc} \parallel R'_{t2} \tag{56}$$

These impedances determine the reflection coefficients at the beginning $\underline{r}_1$ and at the end $\underline{r}_2$ of the MV cable according to (26) and (27). If the termination impedance matches the characteristic impedance $\underline{Z}_c$ of the TL, reflections are minimized. $\underline{Z}_c$ can be calculated with (14) or with the help of the measured S-parameters. For the MV cable used, $\underline{Z}_c \approx 35.5\,\Omega$ and is almost purely ohmic and nearly constant up to 1 GHz.

The amplitude of the generated calibrator pulse u_{cal} depends on the termination resistor R_{t1} connected to its terminals. In Section IV, the calibrator voltage pulse was measured directly at a 50 Ω input channel of an oscilloscope. For simplicity, this impedance-matched voltage pulses of the calibrator were recorded. The following relationship applies between the impedance-matched voltage pulse $u_{cal,50\Omega}$ and the actual pulses at other R_{t1}:

$$u_{cal} = u_{cal,50\Omega} \frac{R_{t1}}{R_{sc}} \tag{57}$$

Thus, before each validation measurement, the initial calibrator PD pulse u_{cal} is calculated for the given R_{t1}. Then the Gaussian pulse model parameters are fitted to u_{cal} to get $u_{cal,m}$. Subsequently (54) is calculated with these PD model parameters. The obtained VSD $\underline{U}_{cal,m}$ is then used as PD source $\underline{U}_s$ of the transmission model.[1] Now (34) or (35) can be solved for the MV cable used. The resulting VSD $\underline{U}_2$ can now be transferred back into the time domain by inverse Fourier transformation in order to obtain the voltage u_2 at the cable end. This voltage can now be compared with the measurement on the oscilloscope.

Fig. 10 shows an example result. For this example, the termination resistor $R_{t1} = 35\,\Omega \approx \underline{Z}_c$ was chosen to avoid reflections. At the other side no additional resistor R'_{t2} was used, i. e. $R_{t2} = 50\,\Omega$. 100 pC pulses were generated by the calibrator. Furthermore $z_s = 0$, $z = l = 10$ m and $\underline{I}_s = 0$ applies.

Transmission model and measurement are similar in time and frequency domain. The remaining deviation can be explained by minor reflections that occur at the discontinuities between the MV cable and the BNC adapters. The characteristic impedance changes at these connections from approximately 35.5 Ω to 50 Ω and minor reflections will occur. However, these reflections are neglected in the transmission model, because $\underline{Z}_c$ and R_{bnc} do not differ much. Apart from these minor deviations, the model is able to predict the transmission behavior of the MV cable well.

B. *Measurement Setup With PD in the Middle of the MV Cable*

This time the calibrator is connected between two pieces of the MV cable, each 10 m long. The measurement setup is shown in Fig. 11. The transmission model is only applicable if both cable sections have a similar characteristic impedance $\underline{Z}_{c1} \approx \underline{Z}_{c2}$. Due to the great similarity in construction, this assumption should be true for most XLPE power cables.

If the calibrator is connected in series between two MV cables, then $u_{cal} \approx u_{cal,50\Omega}$ applies. The rest of the measurement procedure remains the same.

For the example measurement the terminating resistors $R_{t1} = R_{t2} = 33\,\Omega$ were chosen, i. e. an additional resistor $R'_{t2} = 100\,\Omega$ was implemented. Then (35) was solved with

[1]The conversion of a VSD into a logarithmic scale is only done for the diagrams. Mind the index dB.

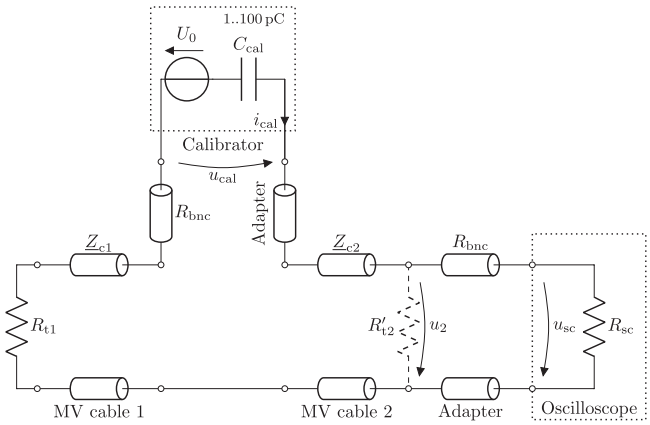

Fig. 11. Measurement setup for the second validation of the transmission model.

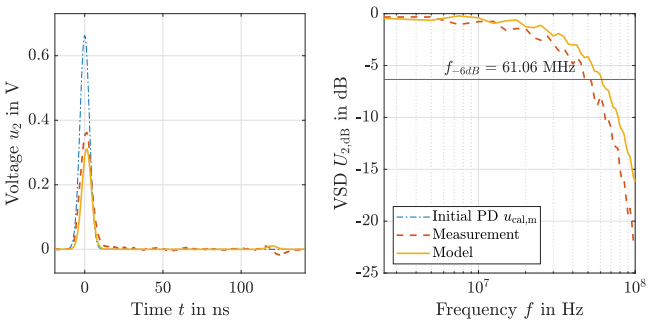

Fig. 12. 100 pC impulse in the middle of 20 m of MV cable in the time and frequency domain with $R_{\mathrm{t1}} = R_{\mathrm{t2}} = 33\,\Omega$.

$z_{\mathrm{s}} = 10\,\mathrm{m}$, $z = l = 20\,\mathrm{m}$ and $\underline{I}_{\mathrm{s}} = 0$. The result is shown in Fig. 12.

Again, the results of the transmission model and measurement are similar in both time and frequency domain. Minor reflections occur at R_{t1} and are measured on the oscilloscope after about 120 ns, which corresponds to about 22 m propagation distance. These reflections due to impedance mismatch are low because the terminating resistors are approximately equal to $\underline{Z}_{\mathrm{c}}$. In the frequency domain, the measurement shows a stronger low-pass behavior compared to the model. This is probably due to longer unshielded cable sections, which could not be avoided in this test setup. All unshielded connections should be kept as short as possible to avoid parasitic inductance. Again, the model is able to predict the transmission behavior of the MV cable well.

The validation results look very promising. Overall it can be concluded that the developed transmission model predicts the propagation behavior of the investigated MV cable with sufficient accuracy. Theoretically, the model should also be valid for cables of any length, since the propagation constant does not change. However, future validation measurements on longer cable sections should provide additional evidence of this.

VI. Conclusion

This article contains an analytical model that describes the transmission of high frequency signals ($f \gg 50\,\mathrm{Hz}$), such as PD, on power cables. The model of this transmission process is based on a derived solution of the telegrapher's equations. In addition to knowing this solution, the propagation constant of the transmission line must also be known. Therefore, a calculation method for the propagation constant of power cables is shown. Using an exemplary MV cable, this method is successfully validated by measurement. The transmission model is then able to reliably predict the propagation and attenuation of various input signals. The signal source can be located anywhere along the cable. This is also confirmed by exemplary measurements with a piece of MV cable and with the help of a PD generator.

It should be mentioned again that all signals with HF spectrum must be treated with the help of the telegrapher's equations. Otherwise all wave phenomena like reflections are neglected.

For the calculation of the propagation constant of the example MV cable, the ohmic and dielectric losses of all cable layers were considered. Compared to previous approaches, the described method is purely analytical and reproducible and considers the frequency dependence of all electrical parameters. Presumably, this calculation method can also be applied to XLPE cables of higher voltages, but this still needs to be investigated.

The transmission model should also be applicable to transmission lines other than power cables if their propagation constant is known.

If multiple XLPE MV cable sections are connected by joints and their characteristic impedance is similar (this should usually be the case), the entire section can be treated as a single cable. Provided that the joints are installed correctly. Minor reflections may occur at the joints, but these should be negligible. In real cable systems, the cable end terminations must also be taken into account. The authors will address these issues in a future publication.

With the help of this model the attenuation and dispersion of transmitted signals can now be easily determined. The remaining spectrum at the measuring point can be simulated accordingly. The authors will use this model in the future to develop methods for detecting PD on MV cables.

References

[1] P. Wagenaars, P. A. F. Wouters, P. J. M. V. D. Wielen, and E. Steennis, "Approximation of transmission line parameters of single-core and three-core XLPE cables," *IEEE Trans. Dielectric Elect. Insul.*, vol. 17, no. 1, pp. 106–115, Feb. 2010.

[2] X. Hu, W. H. Siew, M. D. Judd, A. J. Reid, and B. Sheng, "Modeling of high-frequency current transformer based partial discharge detection in high-voltage cables," *IEEE Trans. Power Del.*, vol. 34, no. 4, pp. 1549–1556, Aug. 2019.

[3] Y. H. M. Thayoob, A. M. Ariffin, and S. Sulaiman, "Analysis of high frequency wave propagation characteristics in medium voltage XLPE cable model," in *Proc. Int. Conf. Comput. Appl. Ind. Electron.*, Kuala Lumpur, Malaysia, Dec. 2010, pp. 665–670.

[4] M. Tozzi, A. Cavallini, G. Montanari, and G. Burbui, "PD detection in extruded power cables: An approximate propagation model," *IEEE Trans. Dielectric Elect. Insul.*, vol. 15, no. 3, pp. 832–840, Jun. 2008.

[5] C. Herold and T. Leibfried, "Advanced signal processing and modeling for partial discharge diagnosis on mixed power cable systems," *IEEE Trans. Dielectric Elect. Insul.*, vol. 20, no. 3, pp. 791–800, Jun. 2013.

[6] J. Steiner, P. Reynolds, and W. Weeks, "Estimating the location of partial discharges in cables," *IEEE Trans. Elect. Insul.*, vol. 27, no. 1, pp. 44–59, Feb. 1992.
[7] G. C. Stone and S. A. Boggs, "Propagation of partial discharge pulses in shielded power cable," in *Proc. IEEE Conf. Elect. Insul. Dielectric Phenomena-Annu. Rep.*, Oct. 1982, pp. 275–280.
[8] C. Herold, "Verfahren zur automatisierten teilentladungsdiagnostik von energiekabeln," Ph.D. dissertation, Karlsruher Institut für Technologie, Karlsruhe, Germany, 2012.
[9] G. Mugala, R. Eriksson, U. Gafvert, and P. Pettersson, "Measurement technique for high frequency characterization of semi-conducting materials in extruded cables," *IEEE Trans. Dielectric Elect. Insul.*, vol. 11, no. 3, pp. 271–280, Jun. 2004.
[10] A. J. Schwab, *Begriffswelt Der Feldtheorie*, 8th ed., Berlin, Heidelberg, Germany: Springer Vieweg, 2019, pp. 185–190.
[11] W. H. Hayt and J. A. Buck, *Engineering Electromagnetics*, (McGraw-Hill Series in Electrical Engineering). Boston, MA, USA: McGraw-Hill, 2001, pp. 301–322.
[12] P. C. J. M. van der Wielen , "On-line detection and location of partial discharges in medium-voltage power cables," Ph.D. dissertation, TU Eindhoven, Eindhoven, the Netherlands, Apr. 2005.
[13] J. Veen, "On-line signal analysis of partial discharges in medium voltage power cables," Ph.D. dissertation, Eindhoven Univ. Technol., Eindhoven, the Netherlands, 2005.
[14] K. C. Gupta, *Computer-Aided Design of Microwave Circuits*. Dedham, MA, USA: Artech, 1981, pp. 30–39.
[15] R. Papazyan, P. Pettersson, H. Edin, R. Eriksson, and U. Gafvert, "Extraction of high frequency power cable characteristics from s-parameter measurements," *IEEE Trans. Dielectric Elect. Insul.*, vol. 11, no. 3, pp. 261–270, Jun. 2004.

Martin Fritsch (Student Member, IEEE) was born in Mühlhausen, Germany, in 1993. He received the B.Eng. degree in electrical engineering from the Frankfurt University of Applied Sciences, Frankfurt, Germany, in 2016, and the M.Sc. degree in electrical engineering from Otto von Guericke University Magdeburg (OVGU), Magdeburg, Germany, in 2018. He is currently a Research Assistant with the Chair of Electric Power Networks and Renewable Energy, OVGU. His research interests include the modeling of electric power systems and the detection of partial discharges.

Martin Wolter (Senior Member, IEEE) was born in Hannover, Germany, in 1981. He received the Diploma, Ph.D. and venia legendi degrees from Leibniz University Hannover, Hannover, Germany in 2006, 2008, and 2012, respectively. For four years, he was the Head of the System Operation Concept Development Team with 50 Hertz Transmission GmbH, Berlin, Germany. Since 2015, he has been the Head of the Chair Electric Power Networks and Renewable Energy, Otto von Guericke University Magdeburg, Magdeburg, Germany. His research interests include modeling and simulation of interconnected electric power systems, development of planning and operation strategies, and multiagent systems.